Fatigue failure maps of heterogeneous materials

François Hild, René Billardon, Anne-Sophie Béranger

Fatigue failure maps of heterogeneous materials

François Hild [a,1], René Billardon [a] Anne-Sophie Béranger [b]

[a] *Laboratoire de Mécanique et Technologie -E.N.S. de Cachan / C.N.R.S. / Université Paris 6-61, avenue du Président Wilson F-94235 Cachan Cedex, France*

[b] *Renault - Direction de la Recherche - Service 0852-860, quai de Stalingrad, F-92109 Boulogne Billancourt, France*

Abstract

In this paper, so-called fatigue failure maps are studied as a function of initial flaw size distributions. The main cause of fatigue failure for brittle materials, and of fatigue initiation for ductile materials, is that initial flaws become critical. Fatigue failure maps where the number of cycles to initiation for a given failure probability is plotted for various flaw size distributions are a means of characterizing the influence of the initial flaw distribution on fatigue crack initiation. The results are applied to fatigue failure of austempered spheroidal graphite cast iron.

Keywords: High cycle fatigue; Failure probability; Flaw distribution; Heterogeneous materials; SG cast iron; Fatigue failure map

1. Introduction

The fatigue process in materials can be schematically divided into two stages. Initiation, which is often due to initial flaws, has to be considered for both brittle and ductile materials. Propagation is usually unstable for brittle materials (e.g. engineering ceramics, many metals in the domain of high cycle fatigue), while stable for ductile materials (e.g. many metals in the domain of low cycle fatigue). In this paper we will focus our attention on initiation in heterogeneous solids. The structure is supposed to remain macroscopically elastic whereas the microscopic evolution of the flaws is described according to a generalized Paris' law up to local failure. The macroscopic initiation corresponds to local failure.

In many heterogeneous materials, initial heterogeneities are mostly sphere-like cavities (e.g. intrinsic flaws in ceramics due to processing, flaws due to cooling down in S.G. cast iron), sphere-like brittle inclusions (e.g. spheroidal graphite), or sphere-like brittle inclusions with low interfacial strength (e.g. in ceramics). In all cases, micro crack initiation appears in planes perpendicular to the maximum principal stress. Furthermore, even though the initial nature of the flaws may be different, as soon as micro initiation occurs, most flaws behave like cracks of surface $\mathcal{A}$ with a normal aligned with the maximum principal stress direction (Clément, 1984). Consequently, in this paper only one flaw population is considered. During micro crack propagation, it is assumed that the surface increases with no morphological change, therefore the radius a of the surface is the only parameter to be accounted for, and the micro crack propagation law will be written in terms of this parameter. Initial heterogeneities are usually randomly distributed within heterogeneous materials, and are modeled by a flaw size distribution f, which is a

[1] Fax: (+33) 1-47-40-22-40; Email: hild@lmt.ens-cachan.fr

function of the size a. This function needs to be determined in order to assess the reliability of heterogeneous materials as shown in Section 2.

The flaws are supposed to be described by cracks whose geometry is taken into account by a dimensionless factor Y such that the energy release rate $\mathcal{G}$ is given by

$$\mathcal{G} = \frac{Y^2\sigma^2 a}{E}, \tag{1}$$

where σ stands for an equivalent uniaxial stress (for instance the maximum principal stress), and E the Young's modulus of the virgin material. It is worth noting that the values of the parameter Y depend upon the geometry of the initial defect and whether this flaw intersects a free surface. For instance, the distance of the flaws to the surface of the structure may be taken into account through the dimensionless parameter Y. Under monotonic and cyclic loading conditions, micro failure can be described by a criterion referring to a critical value of the energy release rate $\mathcal{G}_c$

$$\mathcal{G} \geq \mathcal{G}_c. \tag{2}$$

In order to take into account the localized non-linear behavior of the material in the vicinity of the crack tip under cyclic loading conditions, Elber (1970, 1971) has shown that crack propagation depends upon a so-called effective energy release rate density $\Delta\mathcal{G}_{\text{eff}} = \mathcal{G}_{\max} - \mathcal{G}_{\text{op}}$, where $\mathcal{G}_{\max}$ is the maximum energy release rate over one cycle and $\mathcal{G}_{\text{op}}$ the value of the energy release rate when crack opening occurs. Consequently, it is natural to define a crack initiation criterion as

$$\Delta\mathcal{G}_{\text{eff}} \geq 0. \tag{3}$$

In the following, micro crack initiation is described by a similar criterion postulated by Pellas et al. (1977)

$$\Delta\mathcal{G}_{\text{eff}} = [g(R)]^2\mathcal{G}_{\max} - \mathcal{G}_{\text{th}} \geq 0, \tag{4}$$

where $\mathcal{G}_{\text{th}}$ refers to a so-called threshold energy release rate and $g(R)$ an experimentally identified function of the load ratio R defined as

$$R = \frac{\min_{\text{cycle}}\sigma(t)}{\max_{\text{cycle}}\sigma(t)} = \frac{\sigma_{\min}}{\sigma_{\max}} = \sqrt{\frac{\mathcal{G}_{\min}}{\mathcal{G}_{\max}}}. \tag{5}$$

It is supposed that the load history is simple, i.e. the maximum principal stress direction is constant throughout the load history, and therefore bifurcation is not considered. The micro crack propagation law is assumed to be written as

$$\frac{da}{dN} = G(\Delta\mathcal{G}_{\text{eff}}) \quad \text{when } \Delta\mathcal{G}_{\text{eff}} \geq 0 \text{ and } \mathcal{G} \leq \mathcal{G}_c, \tag{6}$$

where G is a function of the effective energy release rate $\Delta\mathcal{G}_{\text{eff}}$. This function G is known and obtained for macro cracks by performing, for instance, experiments on CT specimens. However, the micro crack propagation law is, a priori, not known, since the average flaw size is, at least, one order of magnitude smaller than the macro crack used in CT specimens. The function G, in addition to the flaw size distribution f, is needed to fully assess the reliability of heterogeneous materials. The identification procedure is addressed in Section 3. The particular micro crack propagation law, as well as flaw size distribution are considered in Section 4 and used in Section 5 to analyze experimental data obtained on an austempered spheroidal graphite cast iron subjected to cyclic loading conditions.

The next step is to study the sensitivity of the failure probability to the flaw size distribution. This constitutes the main aim of this paper and is achieved by deriving so-called *fatigue failure maps* in Section 6. These fatigue failure maps give the number of cycles to initiation, for a given cumulative failure probability and for various flaw size distributions in the material. The approach presented herein may be applied to either brittle materials such as engineering ceramics, or ductile materials such as austempered spheroidal graphite cast iron.

2. Reliability of structures containing flaws

Statistical methods applied to predicting failure under monotonic conditions have been extensively used. The first attempt was made by Weibull (1939) and was based upon a statistical treatment of failure. Monotonic and cyclic loading conditions were analyzed. Batdorf and Crose (1974) modeled initial flaws by cracks whose size and orientation are randomly distributed. Evans and Lamon (1978, 1983, 1988) derived another model based upon similar assumptions. The drawback of these two last approaches is that they are not easily extendable to cases where stable crack

growth is possible (i.e. cyclic conditions). Attempts to model stable crack growth have been made by Sobczyk (1986) using stochastic crack growth equations. Statistical methods are also presently developed for Continuum Damage Mechanics (Krajcinovic, 1989).

In the framework of linear elastic fracture mechanics, Jayatilaka and Trustrum (1977) showed that under some simplifying assumptions the Weibull parameters can be related to the flaw distribution. These results have been extended in the framework of linear elastic fracture mechanics and continuum damage mechanics (Hild and Marquis, 1992). An expression for the cumulative failure probability was obtained in which the flaw distribution was directly considered. Under cyclic conditions, the initial flaw distribution evolves with the number of cycles; however, as shown in Hild and Roux (1991) and recalled in the following, the previous approach can still be used since it deals directly with the flaw distribution.

In the following, for the sake of simplicity, we shall consider only cases for which the load level is constant. Yet generalization to more complex load histories can easily be done by integration of Eq. (6). The cumulative initiation probability, P_{I0}, of a representative volume element (RVE) of volume V_0, is the probability of finding an initial flaw, whose size is larger than the critical flaw size a_c (determined from Eqs. (1) and (2)). In the case of monotonic loading conditions, the expression for P_{I0} is given by

$$P_{I0} = \int_{a_c}^{+\infty} f_0(a)\, da, \tag{7}$$

where f_0 stands for the initial flaw size distribution. In the case of cyclic loading conditions, the stable micro crack propagation leads to the evolution of the flaw size distribution. After N cycles, it is assumed that the flaw distribution is described by a function f_N. The expression for P_{I0} is then given by

$$P_{I0} = \int_{a_c}^{+\infty} f_N(a)\, da. \tag{8}$$

At this stage, it is useful to introduce a function ψ that relates the initial flaw size a_0 to the flaw size after N cycles a_N

$$a_0 = \psi(a_N). \tag{9}$$

The function ψ is determined by integrating Eq. (6). Since the flaw size evolution is assumed to be deterministic, and if the only flaws to cause failure are those initially present within the material, the probability of finding a flaw of size a_N after N cycles is equal to the probability of finding an initial flaw of size $\psi(a_N)$. Thus, the function f_N can be related to the function f_0 by (Hild and Roux, 1991)

$$f_N(a) = f_0(\psi(a)) \frac{\partial \psi}{\partial a}, \tag{10}$$

where the coefficient $(\partial\psi/\partial a)$ comes from the change of measure from da to $d\psi(a)$. Therefore P_{I0} can be rewritten as

$$P_{I0} = \int_{\psi(a_c)}^{+\infty} f_0(a)\, da, \tag{11}$$

where $\psi(a_c)$ denotes the initial flaw size that, after N cycles of loading with a maximum equivalent stress over one cycle σ_{max}, reaches the critical flaw size a_c. Eq. (11) constitutes a unified expression of the cumulative initiation probability in the case of monotonic and cyclic loading conditions. It relates the expression of the cumulative initiation probability to the initial flaw size distribution f_0.

If the interaction between defects is negligible, an independent events assumption can be made. The expression of the cumulative initiation probability, P_I of a structure Ω of volume V can be derived in the framework of the weakest link theory. In the case of monotonic and cyclic loading conditions, the expression of P_I can be related to the cumulative initiation probability, P_{I0}, of a link by (Freudenthal, 1968)

$$P_I = 1 - \exp\left\{ \frac{1}{V_0} \int_{\Omega} \ln(1 - P_{I0})\, dV \right\}. \tag{12}$$

By means of Eqs. (11) and (12), a general relationship between the initial flaw distribution and the cumulative initiation probability of a structure Ω can be derived

$$P_I = 1 - \exp\left\{ \frac{1}{V_0} \int_{\Omega} \ln\left(1 - \int_{\psi(a_c)}^{+\infty} f_0(a)\, da \right) dV \right\}. \tag{13}$$

For monotonic loading conditions, the same equation holds with a_c in place of $\psi(a_c)$. In the case of unstable macro propagation, the structural failure corresponds to the initiation and the expression of the cumulative failure probability P_F is given by

$$P_F = P_I \tag{14}$$

It is worth noting that in the case of high cycle fatigue, the propagation stage tends to become negligible when compared, in terms of number of cycles, with the initiation stage. In such circumstances, Eq. (14) can be applied to both brittle and ductile materials. In other words, since the propagation stage is neglected when Eq. (14) is used, this equation corresponds to a lower bound to the cumulative failure probability of the structure. Hence, in the following, "failure" refers to local failure, i.e. macroscopic initiation or lower bound to macroscopic failure.

Besides, Eqs. (13) and (14) show that the cumulative failure probability is a function of the applied load level, the volume of the structure, the stress field pattern as well as the number of cycles.

3. Identification from *S–N* curves

Standard macroscopic *S–N* curves can be interpreted as iso-failure probability plots. In particular, fatigue limits are defined for different values of the failure probability. In the following, an identification procedure is developed to determine the flaw size distribution f as well as micro crack propagation law modeled by the function G defined in Eq. (6).

When the fatigue limits are known, the identification can be performed in two different steps (Hild and Marquis, 1995). The first step consists in identifying the flaw size distribution f. A minimization scheme is used to determine the minimum error between all the available experimental data on fatigue limits. Such an error can be defined as

$$\mathrm{Err} = \frac{1}{N_e} \sum_{i=1}^{N_e} (P_{Fi} - P_{F\infty})^2 , \tag{15}$$

where N_e denotes the number of experimental data, P_{Fi} is the experimental cumulative failure probability and $P_{F\infty}$ is the predicted cumulative failure probability for an infinite number of cycles to failure. When the number of cycles to failure tends to infinity (i.e. the fatigue limit is reached), the cumulative failure probability can be rewritten as

$$P_{F\infty} = 1 - \exp\left\{ \frac{1}{V_0} \int_{\Omega} \ln\left(1 - \int_{a_{th}(\sigma_F, M)}^{+\infty} f_0(a)\, \mathrm{d}a \right) \mathrm{d}V \right\}, \tag{16}$$

with

$$a_{th}(\sigma_F, M) = \frac{E\mathcal{G}_{th}}{Y^2 \sigma^2_{max}(\sigma_F, M) \left[g(R)\right]^2}, \tag{17}$$

derived from Eqs. (1) and (4), where $\sigma_{max}(\sigma_F, M)$ is the maximum applied equivalent stress level at a point M of Ω when the maximum equivalent stress level in the structure Ω is denoted by σ_F.

The second step of the identification concerns the parameters of the micro crack propagation law G. When the *S–N* curves used for the identification have been obtained in tension, this identification is straightforward: it consists of the analysis of a single iso-cumulative failure probability (e.g. 50%) since an iso-cumulative failure probability is described by a constant cumulative failure probability $P_{F0} = P_{I0}$, therefore $\psi(a_c)$ = const. (see Eq. (11)). When *S–N* curves used for the identification have been obtained for more complex stress fields (e.g. rotating flexure), an iso-cumulative failure probability is no longer associated to a constant cumulative failure probability P_{F0}. However, the identification is still possible by considering an iso-cumulative failure probability (e.g. 50%) defined for the testing specimen considered as a structure.

4. Particularization

In this section, the previous results are particularized to one type of micro crack propagation law as well as to one given flaw size distribution. It is assumed that the flaw size is bounded by a maximum value a_M. Two threshold stresses can be defined. A monotonic threshold stress (this quantity is only relevant in the case of monotonic brittle failure), S_u, may be defined as the lowest value of the stress level below which the monotonic failure probability has a zero value. From

Eqs. (1) and (2), the following expression for S_u can be derived

$$S_u = \frac{1}{Y}\sqrt{\frac{E\mathcal{G}_c}{a_M}}. \tag{18}$$

In other words, S_u denotes the minimum value of the applied local stress for which local failure is certain when a flaw of maximum size a_M is present in an RVE under monotonic loading condition.

In the case of cyclic loading, a cyclic threshold stress may be defined as the lowest value of the stress level below which the cyclic failure probability has a zero value. It is worth noting that this cyclic threshold stress depends upon the load ratio R (see Eq. (4)). For identification purposes, the cyclic threshold stress, S_{th}, is defined for $g(R) = 1$, and is related to the threshold energy release rate $\mathcal{G}_{th}$. Its expression can be derived from Eqs. (1) and (4)

$$S_{th} = \frac{1}{Y}\sqrt{\frac{E\mathcal{G}_{th}}{a_M}}. \tag{19}$$

In other words, S_{th} denotes the minimum value of the applied local stress for which local failure is certain when a flaw of maximum size a_M is present in an RVE under cyclic loading condition. It is worth noting that, combining Eqs. (18) and (19), there exists a simple linear relationship between the two threshold stresses

$$S_{th} = S_u k, \tag{20}$$

with

$$k = \sqrt{\frac{\mathcal{G}_{th}}{\mathcal{G}_c}}. \tag{21}$$

The results derived so far will be used to study the high cycle fatigue behavior of an austempered S.G. cast iron. It is assumed that the micro crack propagation law is a modified version of an Elber law (1970, 1971), and keeps the main features of the macro crack propagation law based upon a generalized Paris' law proposed by Pellas et al. (1977)

$$\frac{da}{dN} = C\left(\frac{\sqrt{\mathcal{G}_{max}}g(R) - \sqrt{\mathcal{G}_{th}}}{\sqrt{\mathcal{G}_c} - \sqrt{\frac{\mathcal{G}_{th}}{g(R)}}}\right)^n, \tag{22}$$

where N denotes the number of cycles, C and n are material parameters. The advantage of Eq. (22) is that it may be integrated explicitly (Hild and Roux, 1991). An expression for the function g has been proposed by Pellas et al. (1977)

$$g(R) = \frac{1-R}{1-mR} \quad \text{if}$$

$$R \le R_c = \frac{\sqrt{\mathcal{G}_{max}} - \sqrt{\mathcal{G}_{th}}}{\sqrt{\mathcal{G}_{max}} - m\sqrt{\mathcal{G}_{th}}}, \tag{23}$$

where m is a material parameter. The values of m are usually on the order of 0.5. The limit value R_c of the load ratio R corresponds to the initiation condition of Eq. (4),

$$\sqrt{\mathcal{G}_{max}}g(R_c) - \sqrt{\mathcal{G}_{th}} = 0, \tag{24}$$

so that

$$\frac{da}{dN} = 0 \quad \text{if } R \ge R_c \text{ and if } \mathcal{G}_{max} < \mathcal{G}_c. \tag{25}$$

For high values of the load ratio R such that $g(R) > k$, unstable propagation is deemed to occur. In practice, that means that when the maximum and minimum stresses over a cycle are of the same order, the initiation conditions correspond to the monotonic failure condition. On the other hand, when the load ratio R is negative, $g(R)$ remains close to unity. The approximation $g(R) \approx 1$ is usually sufficient to model the effects of negative load ratios.

By integration of Eq. (22) and recalling Eq. (1), the following closed form solution can be derived (Hild and Roux, 1991)

$$\varphi\left(\sqrt{\frac{a_N}{a_M}}\right) - \varphi\left(\sqrt{\frac{a_0}{a_M}}\right) = C^*\left(\frac{g(R)}{1 - \frac{\sqrt{\mathcal{G}_{th}}}{\sqrt{\mathcal{G}_c}g(R)}}\right)^n \left(\frac{\sigma}{S_u}\right)^n N, \tag{26}$$

where a_M denotes the maximum flaw size in the structure, a_0 the initial flaw size, and a_N the flaw size after N cycles. The dimensionless constant C^* is equal to C/a_M. When a_N is equal to the critical flaw size a_c determined from the failure criterion defined in Eq. (2), the initial flaw size is then equal to the initial critical flaw size $\psi(a_c)$ and Eq. (26) allows to relate $\psi(a_c)$ to a_c by

$$\varphi\left(\sqrt{\frac{a_c}{a_M}}\right) - \varphi\left(\sqrt{\frac{\psi(a_c)}{a_M}}\right) = C^* \left(\frac{g(R)}{1 - \frac{\sqrt{\mathcal{G}_{th}}}{\sqrt{\mathcal{G}_c} g(R)}}\right)^n \left(\frac{\sigma}{S_u}\right)^n N_F, \quad (27)$$

where N_F denotes the number of cycles to failure. The value of the function φ depends upon the power n. When $n \neq 1$ and $n \neq 2$, the function φ is given by

$$\varphi(x) = \varphi\left(\sqrt{\frac{a}{a_M}}\right) = 2\frac{(x - x_{th})^{1-n}(x_{th} - (n-1)x)}{(n-1)(n-2)}, \quad (28)$$

where x_{th} is the normalized threshold defect size obtained by using Eqs. (17) and (19)

$$x_{th} = \sqrt{\frac{a_{th}}{a_M}} = \frac{S_{th}}{\sigma g(R)} \quad (29)$$

At an RVE level, an iso-probability is defined as a curve σ–N such that the cumulative failure probability $P_{F0} = P_{I0}$ is constant. If the load history is proportional, it can be shown from Eq. (11) that this condition can be rewritten as

$$\frac{\psi(a_c)}{a_M} = B, \quad (30)$$

where the constant B depends upon the details of the flaw distribution and the value of the considered cumulative failure probability. By using Eqs. (27), (30) the normalized number of cycles to failure N^* is given by

$$N^* = +\infty \quad \text{if } \sigma\, g(R)\sqrt{B} < S_{th} \quad (31.1)$$

$$N^* = \left(\frac{1 - \frac{k}{g(R)}}{g(R)}\right)^n \left(\frac{\sigma}{S_u}\right)^{-n} \times \left\{\varphi(S_u/\sigma) - \varphi(\sqrt{B})\right\} \quad \text{if } \frac{S_{th}}{g(R)} \leq \sigma\sqrt{B} \leq S_u \quad (31.2)$$

$$N^* = 0 \quad \text{if } \sigma\sqrt{B} > S_u, \quad (31.3)$$

where the normalized number of cycles to failure is defined as

$$N^* = C^* N_F. \quad (31.4)$$

Eq. (31.1) corresponds to a case where no failure at all is possible. The limiting case is when $\sigma g(R)\sqrt{B} = S_{th}$, in other words, the "fatigue limit" is reached. The expression of the cumulative failure probability then only depends upon the initial flaw distribution and the value of the cyclic threshold stress S_{th}. This case allows an identification of the flaw size distribution independently of the crack growth law (as presented in Section 3). Eq. (31.2) corresponds to a case where fatigue failure occurs. For a given value of B (i.e. a given failure probability), the evolution of the number of cycles to failure mainly depends on the crack growth law. Therefore, the analysis of a constant failure probability allows to identify the parameters of the crack growth law, provided the flaw size distribution is known (i.e. the different values of the constant B have been identified). When this approach is still applicable to smaller number of cycles to failure, Eq. (31.3) corresponds to a case where monotonic failure occurs. The limiting case is when $\sigma\sqrt{B} = S_u$. The expression of the cumulative failure probability again only depends upon the initial flaw distribution, and the value of the monotonic threshold stress S_u.

Lastly, it is assumed that the flaw size distribution f_0 can be particularized as a beta distribution

$$f_0(a) = \frac{a_M^{-1-\alpha-\beta}}{B_{\alpha\beta}} a^\alpha (a_M - a)^\beta, \quad 0 < a < a_M, \quad \alpha, \beta > -1, \quad (32)$$

where α and β are the parameters of the beta function, and $B_{\alpha\beta}$ is equal to $B(\alpha+1, \beta+1)$, where $B(.,.)$ is the Euler function of the first kind (Spanier and Oldham, 1987). In Fig. 1, the normalized beta density and cumulative beta density are plotted with $\alpha = 1.8$, $\beta = 17.5$ and are compared with the case when $\alpha = 1$, $\beta = 5$. Fig. 2 shows a Wöhler diagram when $\alpha = 1$, $\beta = 5$, $R = 0$, $n = 4$, and $k = 1/3$. It is recalled that $N^* = C^* N_F$ is the normalized number of cycles to failure. It is worth noting that when the ratio $\sigma/S_u < 1$, no failure occurs under monotonic condition while failure due to cyclic loading occurs when $\sigma/S_{th} \geq 1$, $\sigma/S_u \geq k = 1/3$. When $\sigma/S_{th} < 1$, no failure at all is possible. These results are consistent with the two

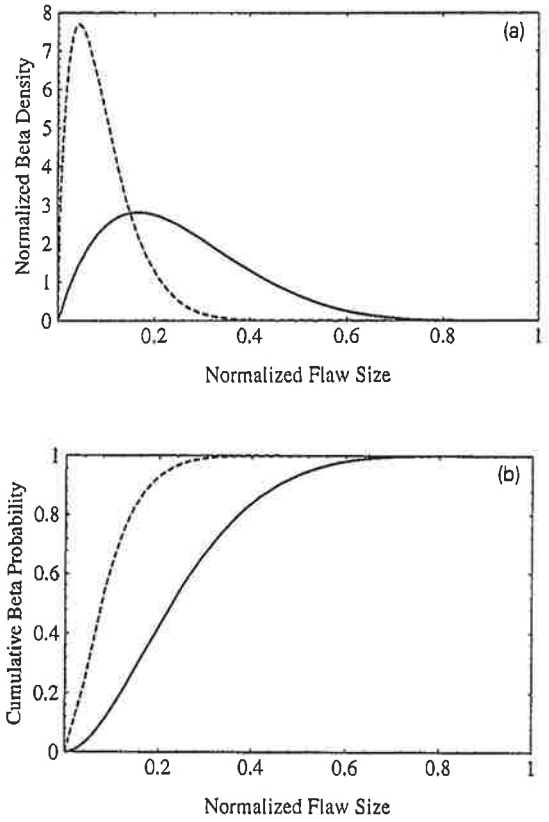

Fig. 1. (a) Beta density and (b) cumulative probability when $\alpha = 1$ and $\beta = 5$ (solid line), and $\alpha = 1.75$ and $\beta = 17.5$ (dashed line).

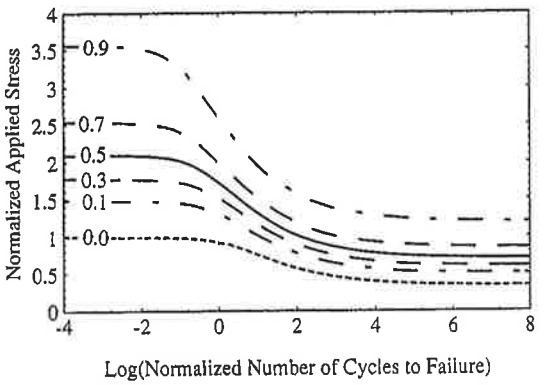

Fig. 2. Wöhler diagram when $\alpha = 1$, $\beta = 5$, $R = 0$, $n = 4$, and $k = 1/3$. Evolution of the normalized applied stress, σ/S_u, as a function of the normalized number of cycles, N^*, for different cumulative failure probabilities, P_{F0}.

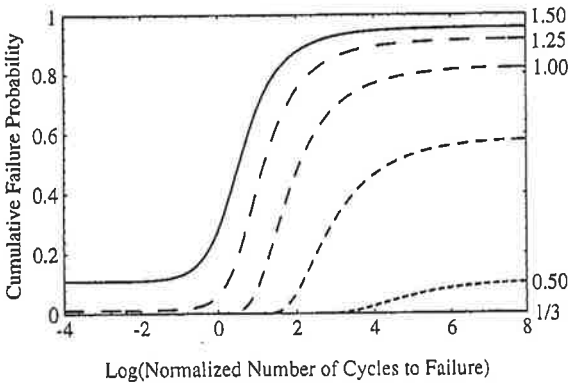

Fig. 3. Evolution of the cumulative failure probability, P_{F0}, as a function of the normalized number of cycles, N^*, for different values of the stress level, σ/S_u, when $\alpha = 1$, $\beta = 5$, $R = 0$, $n = 4$, and $k = 1/3$. Evolution of the cumulative failure probability, P_{F0}, as a function of the normalized number of cycles, N^*, for different values of the stress level, σ/S_u, when $\alpha = 1$, $\beta = 5$, $R = 0$, $n = 4$, and $k = 1/3$.

threshold stresses S_u and $S_{th} = kS_u$ defined in Eqs. (18) and (19).

By using Eq. (31.2), the equation of the median Wöhler curve ($P_{F0} = 50\%$), if $S_{th}/g(R) \leq \sigma\sqrt{B_{50}} \leq S_u$, is given by

$$N_{50}^* = \left(\frac{1 - \dfrac{\sqrt{\mathcal{G}_{th}}}{\sqrt{\mathcal{G}_c g(R)}}}{g(R)} \right)^n \left(\frac{\sigma}{S_u} \right)^{-n} \times \left\{ \varphi(S_u/\sigma) - \varphi(\sqrt{B_{50}}) \right\}, \tag{33}$$

where B_{50} denotes the value of B for which $P_{F0} = 50\%$. This equation can also be written in a format close to that suggested by Wöhler

$$\log(N_{50}^*) = \zeta\left(\frac{\sigma}{S_u}; R; n \right) - n\frac{\sigma}{S_u}, \tag{34}$$

where ζ is a function of the normalized stress level σ/S_u, the load ratio R, and n, the power of the crack growth law. The fatigue limit, S_{50}, defined as the smallest value of the stress level such that $P_{F0} = 50\%$

$$S_{50} = \frac{S_{th}}{g(R)\sqrt{B_{50}}} \tag{35}$$

In Fig. 3, the cumulative failure probability is plotted as a function of the normalized number of cycles to failure, N^*, for different stress levels when $R = 0$.

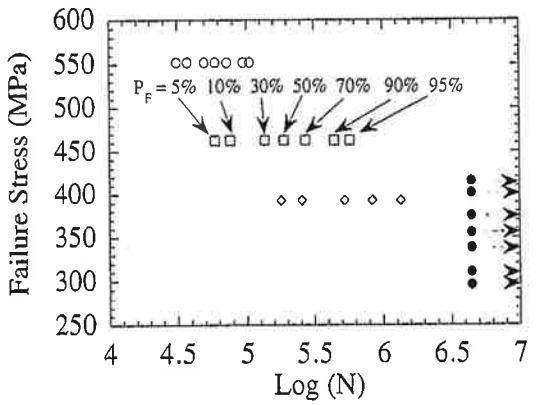

Fig. 4. Experimental data of austempered nodular graphite cast iron subjected to rotating flexure.

All these results show that the scatter observed in fatigue can be described by the introduction of a statistical flaw size distribution.

5. Analysis of fatigue tests on austempered S.G. cast iron

In this section, a series of experiments reported in Jokipii (1992) are analyzed in detail. These experiments have been carried out at different stress levels on Kymenite, which is an austempered S.G. cast iron, grade K-10005. The ratio between the threshold energy release rate and the critical energy release rate is of the order of 1/9 (i.e. $k = 1/3$). The specimens were subjected to rotating flexure with a test area diameter equal to 7.5 mm. Fig. 4 shows the experimental data obtained in rotating flexure. It is worth noting that there is information on both limited (open symbols) and unlimited (solid symbols) number of cycles to failure at different stress levels and for different cumulative failure probabilities.

In this case a two-step identification procedure can be carried out. The following values are identified by analyzing the fatigue limits: $\alpha = 1.8$, $\beta = 17.5$, $V/V_0 = 112$, $S_u = 520$ MPa. The result of the identification is shown in Fig. 5 in terms of cumulative failure probability versus fatigue limit. In flexure, because of the stress heterogeneity in the specimen, Eq. (30) is not equivalent to an iso-cumulative failure probability on a structural level. One single iso-cumulative failure probability is still sufficient to identify the two material parameters. The iso-cumulative failure probability

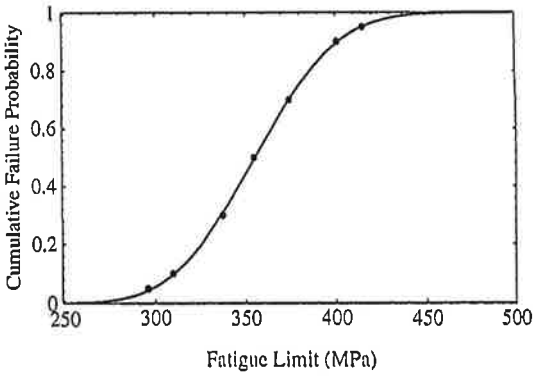

Fig. 5. Experiments and predictions of the fatigue limits for different cumulative failure probabilities ($\alpha = 1.75$, $\beta = 17.5$, $V/V_0 = 112$, $S_u = 520$ MPa, $k = 1/3$).

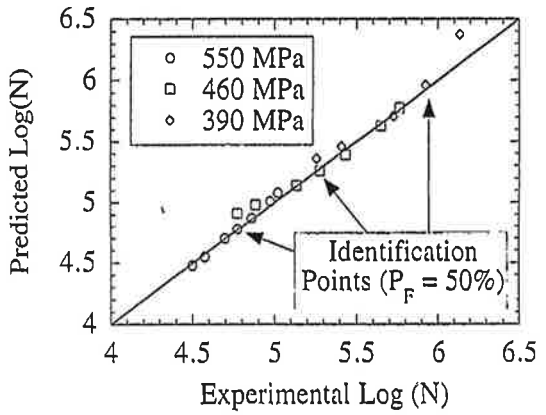

Fig. 6. Comparisons between experimental and predicted values of the number of cycles to failure when $k = 1/3$ ($n = 2.34$, and $C/a_M(1-k)^n = 1.3 \times 10^{-4}$). The identification points were taken for a cumulative failure probability equal to 50%.

of 50% is used to minimize an error similar to that defined in Eq. (15). The following values were obtained: $n = 2.34$, and $C/a_M(1-k)^n = 1.3 \times 10^{-4}$. In Fig. 6 the predictions of the number of cycles to failure are compared with the experimental observations. Three points were used for the identification and the remaining points are predictions. Out of 19 experimental data, 15 points exhibit a difference between experimental and predicted value of less than 15%, and the maximum difference is 75%. In Fig. 7 the cumulative failure probability is plotted as a function of the number of cycles to failure for the three different stress levels. It is worth noting that all the predictions are in good agreement with the experimental data.

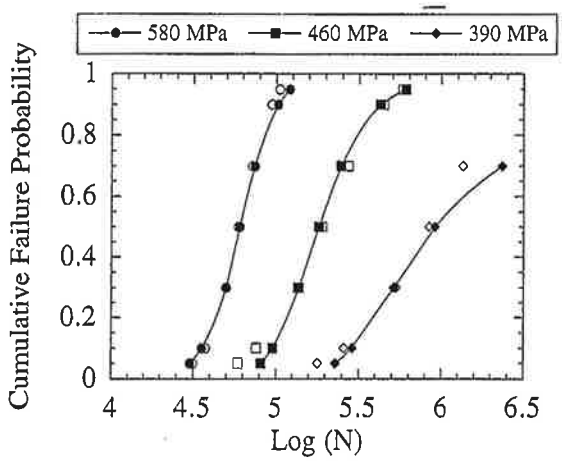

Fig. 7. Comparisons between experimental and predicted values of the cumulative failure probability for three different stress levels (550, 460, and 390 MPa), open symbols are experiments and solid symbols are the predictions.

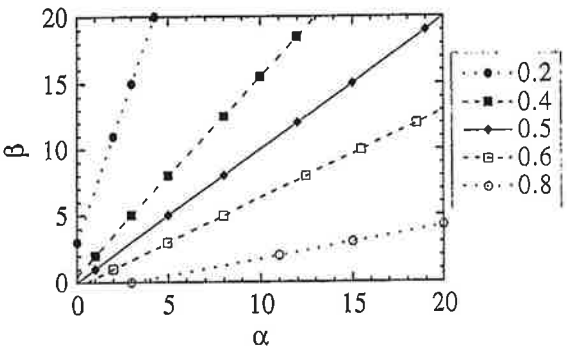

Fig. 8. Evolution of the average flaw size, $\bar{a}/a_M$, as a function of the parameters α and β.

6. Fatigue failure maps

The next question to address is the influence of the flaw size distribution upon failure properties. So-called fatigue failure maps are drawn for this purpose. By varying the values of α and β of the beta distribution given in Eq. (32), it is possible to vary the values of the average flaw size and the corresponding standard deviation. Fig. 8 shows the type of dependence of the average flaw size upon the values of the parameters α and β. For a beta density (Spanier and Oldham, 1987), the average flaw size, $\bar{a}$ is given by

$$\frac{\bar{a}}{a_M} = \frac{\alpha+1}{\alpha+\beta+2} \tag{36}$$

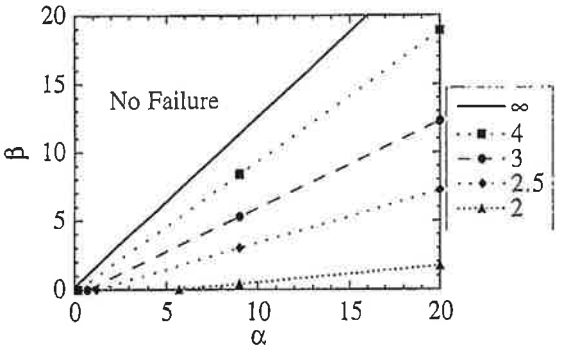

Fig. 9. Fatigue failure maps giving the logarithm of the normalized number of cycles to failure as a function of the parameters α and β, for a given cumulative failure probability P_{F0} = 50%, and a given load level $\sigma/S_u = 0.5$, $R = 0$, $n = 4$, and $k = 1/3$.

and the corresponding standard deviation $\bar{\bar{a}}$

$$\frac{\bar{\bar{a}}}{a_M} = \sqrt{\frac{(\alpha+1)(\beta+1)}{(\alpha+\beta+2)^2(\alpha+\beta+3)}}. \tag{37}$$

Fatigue failure maps correspond to various contours of number of cycles to failure for a fixed stress level and are drawn for a given value of the cumulative failure probability $P_{F0} = P_{I0}$. Therefore they directly illustrate the relationship between the flaw size distribution in the material and the reliability of heterogeneous materials under cyclic loading conditions.

The first stage is to determine the values of the constants B for different values of α and β to plot such a map for a given value of P_{F0}, for instance, 50%. In the following, we shall consider cases for which $0 \leq \alpha, \beta \leq 20$, and all these results are given for $R = 0$, and are easily generalized to other cases. To obtain the number of cycles to failure when P_{F0} = 50%, we use Eqs. (31.1), (31.2) and (31.3). One of these maps is drawn in Fig. 9 for a load level characterized by the ratio $\sigma/S_u = 0.5$. The boundary of the no-failure zone corresponds to $\sigma\sqrt{B_{50}} = S_{th}$ (since $g(R) = 1$). When the failure probability equals 50%, this boundary can be described by a straight line. Because initiation and final failure are assumed to be described by the same kind of criterion referring to the energy release rate $\mathcal{G}$, the boundaries can be drawn on one single map. These boundaries can be drawn for different stress levels, as shown in Fig. 10. Such a map can be used as follows. Below a given normalized stress level contour, σ/S_u, monotonic failure occurs when P_{F0} = 50% and Eq.

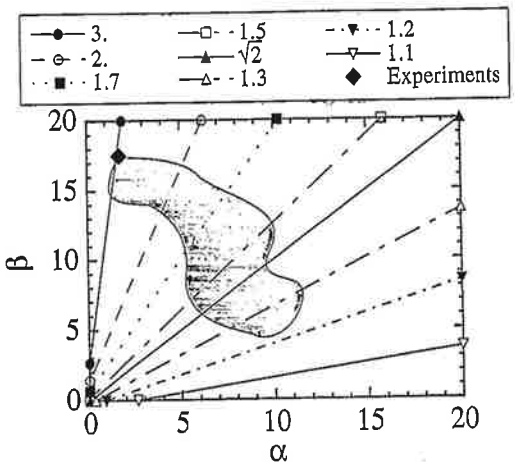

Fig. 10. Fatigue gfailure map giving the boundary of the monotonic failure and no-failure zones as a function of the parameters α and β when P_{F0} =50% for different normalized stress levels σ/S_u or $\sigma g(R)/S_{th}$.

(31.3) is satisfied. Above a given normalized stress level contour $\sigma g(R)/S_{th}$, no failure takes place when P_{F0} = 50% and Eq. (31.1) is satisfied.

When comparing Figs. 8, 9, and 10 it can be noticed that the iso-number of cycles to failure has the same shape as the average defect size curves; this can be explained by the fact that the iso-probability P_{F0} = 50% is approximately given by a constant value of $(\alpha+1)/(\alpha+\beta+2)$, i.e. $\bar{a}/a_M$ = const. (Eq. (36)). This also means that for this particular iso-probability the number of cycles to failure is weakly influenced by the standard deviation $\tilde{a}$.

Another feature of Eq. (12) is that the considered stress field is the macroscopic stress field since the interactions between defects are neglected. This approach can therefore be used as a post-processor to any classical structural analysis (performed on the structure without flaws). Phenomena such as volume effects and stress heterogeneity effects which have been modeled by Eq. (12) in the case of monotonic failure (Freudenthal, 1968; Hild et al., 1992), may also be modeled by this approach and applied to fatigue failure.

7. Conclusions

A reliability analysis taking account of flaw size distributions has been developed for solids subjected to cyclic loading conditions. Emphasis is put on the initiation stage, which is directly related to the evolution of initial flaws. A unified expression of the cumulative failure probability is derived for cyclic and monotonic failure within the framework of the weakest link theory and by assuming that flaws do not interact.

A two-step procedure is developed to identify the flaw distribution as well as the parameters of the micro crack propagation law. It is shown that the identification of the parameters related to flaw size distribution and crack growth law can be decoupled. In particular, the value of the parameters of the flaw size distribution can be determined from the fatigue limits at different failure probabilities. The identification of the parameters of the crack growth law can be obtained by the analysis of one single iso-cumulative failure probability (say 50%).

General features observed in the case of high cycle fatigue are modeled. For instance, a Wöhler diagram is drawn for different failure probabilities. Experiments on austempered S.G. cast iron are analyzed within the previous framework. The identification strategy is applied to experimental data in rotating flexure. The predictions of the whole set of data are in good agreement with the experimental number of cycles to failure. This last result shows that the expression of cumulative failure probability proposed herein is able to model fatigue data obtained on austempered S.G. cast iron.

To model the effect of initial flaw distributions on the fatigue behavior of heterogeneous materials, fatigue failure maps are introduced. They consist in plotting contours of constant number of cycles to failure in a space representative of the initial flaw distributions. Such maps are drawn at a given load level and for a given cumulative failure probability. When the initial flaw distribution is modeled by a beta distribution of exponents α and β, the maps are drawn in an α–β plane. The fatigue failure maps allow the extrapolation of the results obtained for a given flaw size distribution to other flaw size distributions.

Typical application of this approach concerns the reliability analysis of casted components. More and more tools are available to predict the different flaw size distributions from one point of a part of a cast to another, whereas the fatigue behavior of the material is in general merely derived from experiments performed on so-called flawless specimens. A fatigue failure map representative of the sensitivity of the material to flaws will enable a prediction of the reliability of the whole

component under cyclic loading conditions; in other words, it will enable the prediction of the number of cycles to macro crack initiation, or the probability of reaching a certain number of cycles without failure at every point of the component.

Acknowledgements

The authors gratefully acknowledge the financial support of Renault through contract CNRS/109 (H5-24-12) with the Laboratoire de Mécanique et Technologie, Cachan.

References

Batdorf, S. B. and J. G. Crose (1974), A statistical theory for the fracture of brittle structures subjected to polyaxial stress states, *J. Appl. Mech. 41*, 459-465.

Clément, P. (1984), Propagation par fatigue de petits défauts dans une fonte G.S., mémoire CNAM Paris.

Elber, W. (1970), Fatigue crack closure under cyclic tension, *Eng. Fract. Mech.* 2, 37-45.

Elber, W. (1971), *The Significance of Fatigue Crack Closure*, American Society for Testing and Materials, STP 486, Philadelphia, pp. 230-242.

Evans, A. G. (1978), A General approach for the statistical analysis of multiaxial fracture, *J. Am. Ceram. Soc. 61(7-8)*, 302-308.

Freudenthal, A. M. (1968), *Statistical Approach to Brittle Fracture*, Academic Press, pp. 591-619.

Hild, F. and S. Roux (1991), Fatigue initiation in heterogeneous brittle materials, *Mech. Res. Comm. 18 (6)*, 409-414.

Hild, F., R. Billardon and D. Marquis (1992), Hétérogénéité des contraintes et rupture des matériaux fragiles, *C.R. Acad. Sci. Paris, t. 315 (Série II)*, 1293-1298.

Hild, F. and D. Marquis (1992), A statistical approach to the rupture of brittle materials, *Eur. J. Mech. A 11(6)*, 753-765.

Hild, F. and D. Marquis (1995), Fiabilité de matériaux avec défauts en propagation stable, *C.R. Acad. Sci. Paris, t. 320 (Série IIb)*, 57-62.

Jayatilaka, A. D. S. and K. Trustrum (1977), Statistical approach to brittle fracture, *J. Mater. Sci. 12*, 1426-1430.

Jokipii, K., (1992), Kymenite, austempered ductile iron as material for various applications, in: *Eur. Meeting on Castings in Austempered Spheroidal Graphite Cast Iron*, Centre Technique des Industrie de la Fonderie, Sèvres (France).

Krajcinovic, D. (1989), Damage Mechanics, Mech. Mat., 8, 117-197.

Lamon, J. and A. G. Evans (1983), Statistical analysis of bending strengths for brittle solids: a multiaxial fracture problem, *J. Am. Ceram. Soc. 66*, 177-182.

Lamon, J. (1988), Statistical approaches to failure for ceramic reliability assessment, *J. Am. Ceram. Soc. 71(2)*, 106-112.

Pellas, J., G. Baudin and M. Robert (1977), Mesure et calcul du seuil de fissuration après surcharge, *Recherche aérospatiale 3*, 191-201.

Sobczyk, K. (1986), Modelling of random fatigue crack growth, *Eng. Fract. Mech. 24(4)*, 609-623.

Spanier, J. and K. B. Oldham (1987), *An Atlas of Functions*, Springer Verlag, New York.

Weibull, W. (1939), A statistical theory of the strength of materials, *Roy. Swed. Inst. Eng. Res.* 151.